JOC*Article*

Diastereomers of *N*-α-Phenylethyl-*t*-butylsulfinamide: Absolute Configurations and Predominant Conformations

Ana G. Petrovic,[†] Prasad L. Polavarapu,*[,†] Jozef Drabowicz,[‡,||] Piotr Łyżwa,[‡] Marian Mikołajczyk,[‡] Wanda Wieczorek,[§] and Agnieszka Balińska[||]

Department of Chemistry, Vanderbilt University, Nashville, Tennessee 37235, Center of Molecular and Macromolecular Studies, Polish Academy of Sciences, Sienkiewicza 112, 93-236 Lodz, Poland, Institute of General and Ecological Chemistry, Technical University of Lodz, 90-924, Lodz, Zeromskiego 116, Poland, Jan Długosz University, Institute of Chemistry and Environmental Protection, al. Armii Krajowej 13/15, 42-201 Częstochowa, Poland

Prasad.L.Polavarapu@vanderbilt.edu

Received November 27, 2007

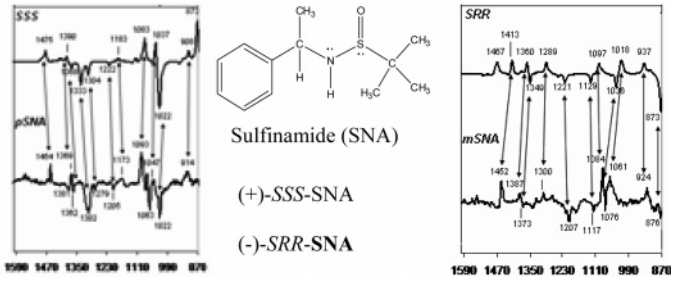

N-α-Phenylethyl-*t*-butylsulfinamide is a complicated system for determining molecular stereochemistry because of numerous possibilities for assigning the absolute configuration and a predominant conformation. Two diastereomers of *N*-α-phenylethyl-*t*-butylsulfinamide derived from (−)-(*S*)-α-phenylethyl amine, a (+)-diastereomer and a (−)-diastereomer, have been synthesized and their experimental chiroptical spectroscopic properties have been measured. These properties include vibrational circular dichroism, electronic circular dichroism and optical rotatory dispersion. Using these experimental data, in conjunction with corresponding density functional theoretical predictions, the absolute configuration and predominant conformations of these two diastereomers have been determined. Also, the absolute configuration of (−)-diastereomer has been independently confirmed by determining its structure from X-ray diffraction data.

Introduction

Within the family of sulfinyl derivatives,[1,2] chiral sulfinamides serve as useful chiral building blocks. In the enantioselective asymmetric synthesis of many organic compounds, which are important for the development of active pharmaceutical ingredients and intermediates, sulfinamides were used as efficient chiral auxiliaries[3−6] and catalysts.[7,8] They found applications in the synthesis of enantiopure sulfinimines[1,4,9,10] as precursors for α- and *β*-amino acids,[4,10−12] α- and *β*-aminophosphonates,[13,14] and chiral amines.[15,16] Sulfonamides, obtained from oxidation of sulfinamides,[17] have been suggested[18] to have

* Corresponding author. Phone: (615)322-2836. Fax: (615)322-4936.
[†] Vanderbilt University.
[‡] Polish Academy of Sciences.
[§] Technical University of Lodz.
[||] Jan Długosz University.

(1) Mikolajczyk, M.; Drabowicz J.; Kielbasinski, P. *Chiral Sulfur Reagents: Applications and Aymmetric and Stereoselective Synthesis*; CRC Press: New York, 1997.
(2) Metzner, P.; Thuillier, A. *Sulfur Reagents in Organic Synthesis*; Academic Press: London, 1994.
(3) Senanayake, C. H.; Krishnamurthy, D.; Lu, Z.; Han, Z.; Gallou, I. *Aldrichim. Acta* **2005**, *38*(3), 93−104.
(4) Davis, F. A.; Zhou, P.; Chen, B. *Chem. Soc. Rev.* **1998**, *27*, 13−18.
(5) Evans, D. A.; Faul, M. M.; Colombo, L.; Bisaha, J. J.; Clardy, J.; Cherry D. *J. Am. Chem. Soc*. **1992**, *114*, 5977−5985.
(6) Davis, F. A.; Liu, H.; Zhou, P.; Fang, T.; Reddy, G. V.; Zhang, Y. *J. Org. Chem.* **1999**, *64*, 7559−7567.
(7) Pei, D.; Wang, Z.; Wei, S.; Zhang, Y.; Sun, J. *Org. Lett.* **2006**, *8* (25), 5913−5915.
(8) Ellman, J. A. *Pure Appl. Chem.* **2003**, *75*, 39−46.
(9) Davis, F. A.; Reddy, R. E.; Szewczyk, J. M.; Reddy, C. V.; Portonovo, P. S.; Zhang, H.; Fanelli, D.; Reddy, R. T.; Zhou, P.; Carroll, Patrick. *J. Org. Chem*. **1997**, *62*, 2555−2563.
(10) Davis, F. A.; Fanelli, D. L. *J. Org. Chem.* **1998**, *63*, 1981−1985.

10.1021/jo702544g CCC: $40.75
Published on Web 03/15/2008

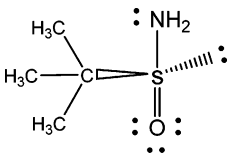

FIGURE 1. *t*-Butanesulfinamide (**1**).

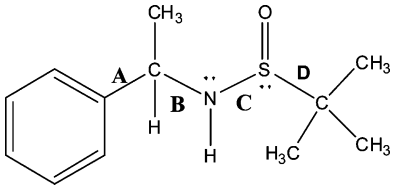

FIGURE 2. The chemical structure of *N*-α-phenylethyl-*t*-butylsulfinamide (**2**).

applications in medicinal chemistry. Peptidosulfinamide, a sulfinamide derivative, has found application[19] for the development of HIV protease inhibitors.

The selective induction of chirality through asymmetric reactions necessitates not only the synthesis of enantiopure sulfinamides, but also the reliable determination of their absolute stereochemistry. In recent years, chiroptical spectroscopic methods[20] are becoming invaluable tools for reliable determination of absolute configuration and conformations of different types of chiral molecules. This accomplishment is made possible by the advances in instrumentation for experimental measurements, and in quantum theoretical methods for theoretical prediction, of chiroptical spectroscopic properties. The chiroptical spectroscopic methods used in the present study are vibrational circular dichroism (VCD), electronic circular dichroism (ECD), and optical rotatory dispersion (ORD).

Recently, we have explored the applicability of chiroptical spectroscopic methods for structural elucidation of chiral sulfinamides by investigating one of the simplest sulfinamides, *t*-butanesulfinamide, **1** (Figure 1). Consistent and unambiguous stereochemical assignment was obtained[21] for **1** using all three chiroptical spectroscopic methods.

N-α-Phenylethyl-*t*-butylsulfinamide, **2** (Figure 2) is a complicated system for determining molecular stereochemistry. This is because conformational flexibility resulting from four rotatable bonds (Figure 3) leads, at least in principle, to $3^4 = 81$ conformers. Furthermore, if one assumes a possibility of the existence of a stereogenic nitrogen atom, three stereogenic centers (C, N, S) of **2** lead to $2^3 = 8$ possible diastereomers (Figure 4). As a result, one has to consider $81 \times 8 = 648$ possibilities for predicting the chiroptical properties and assigning the absolute configuration and predominant conformations of **2**. In practice, however, this number of possibilities is reduced, as three of the orientations each for benzene and *t*-butyl groups can be reduced to two, each due to the planarity of the benzene ring and the symmetry of the *t*-butyl group (vide infra). Furthermore, four diastereomers are mirror images of the other four. Therefore it is sufficient to do calculations on four diastereomers, each with 36 possible conformations.

In the present work, two diastereomers of **2**, a (+)-diastereomer (*pSNA*-**2**) and a (−)-diastereomer (*mSNA*-**2**) have been synthesized in the reaction of racemic *t*-butanesulfinyl chloride and (−)-(*S*)-α-phenylethyl amine, and their experimental chiroptical spectroscopic properties have been measured. Using these experimental data, in conjunction with corresponding density functional predictions, the absolute configuration and predominant conformations of these two diastereomers having the opposite absolute configurations at the stereogenic sulfinyl sulfur atoms have been determined. Also the absolute configurations at the stereogenic carbon and sulfur atoms of *mSNA*-**2** are independently confirmed here by determining its structure from X-ray diffraction data.

It should be noted here that two diastereomers of the sulfinamide **2** having the (*R*) absolute configuration at the stereogenic sulfinyl sulfur atom have very recently been prepared by the reduction of optically active *N*-*t*-butylsulfinylimine derived from the enantiomerically pure sulfinamide (*R*)-**1** and acetophenone.[22a] They were isolated also earlier as the products of an asymmetric addition of methylmagnesium bromide to optically active *N*-*t*-butylsulfinylimine derived from the enantiomerically pure sulfinamide (*R*)-**1** and benzaldehyde.[22b]

It should be mentioned that the structural conclusions obtained here from chiroptical spectroscopic data and X-ray data were not disclosed to individual research groups working on these analyses until this manuscript was prepared. Therefore the structural conclusions obtained from chiroptical spectroscopic data and X-ray data are truly independent, and such independent establishment of stereochemistry from chiroptical spectroscopic data reflects the reliability and importance of modern day chiroptical spectroscopies in molecular stereochemistry.

Results and Discussion

As mentioned in the introduction, the presence of three stereogenic atoms C, N, and S in **2** leads to eight possible diastereomers. However, since four of the diastereomers are mirror images of the other four, only one set of non-enantiomeric diastereomers need to be investigated. This is because chiroptical spectra of the second set of diasteromers are obtained by multiplying those of the first set by −1. The four diastereomers selected as theoretical models for geometry optimization and chiroptical predictions are *SSS*, *SRS*, *SSR*, and *SRR*. The three-letter designations represent configurational assignment at the stereogenic atoms C, N, and S, respectively.

Investigations[21] on a smaller sulfinamide **1** revealed that neither the geometries nor relative electronic energies are

(11) Davis, F. A.; Szewczyk, J. M. *Tetrahedron Lett.* **1998**, *39*, 5951−5954.
(12) Davis, F. A.; Szewczyk, J. M.; Reddy, R. E. *J. Org. Chem.* **1996**, *61*, 2222−2225.
(13) Lefebvre, I. M.; Evans, S. A. *J. Org. Chem.* **1997**, *62*, 7532−7533.
(14) Mikolajczyk, M.; Lyzwa, P.; Drabowicz, J. *Tetrahedron: Asymmetry* **1997**, *8* (24), 3991−3994.
(15) Han, Z.; Krishnamurthy, D.; Pflum, D.; Grover, P.; Wald, S. A.; Senanayake, C. H. *Org. Lett.* **2002**, *4* (23), 4025−4028.
(16) Moreau, P.; Essiz, M.; Merour, J.; Bouzard, D. *Tetrahedron: Asymmetry*. **1997**, *8* (4), 591−598.
(17) Clennan, E. L.; Chen, M.; Greer, A.; Jensen, F. *J. Org. Chem.* **1998**, *63*, 3397−3402.
(18) Bharatam, P. V.; Kaur, A.; Kaur, D. *J. Phys. Org. Chem.* **2002**, *15*, 197−203.
(19) Moree, W. J.; Van der Marel, G. A.; Liskamp, R. J. *J. Org. Chem.* **1995**, *60*, 5157−5169.
(20) For recent reviews, see (a) Polavarapu, P. L. *Chem. Rec.* **2007**, *7*, 125−136. (b) Polavarapu, P. L. *Int. J. Quantum Chem.* **2006**, *106*, 1809−1814.
(21) Petrovic, A. G.; Polavarapu, P. L. *J. Phys. Chem. A* **2007**, *111*, 10938−10943.
(22) (a) Tanuwidjaja, J.; Peltier, H. M.; Ellman, J. A. *J. Org. Chem.* **2007**, *72*, 626−629. (b) Cogan, D. A.; Liu, G.; Ellman, J. A. *Tetrahedron*, **1999**, *55*, 8883−8904.

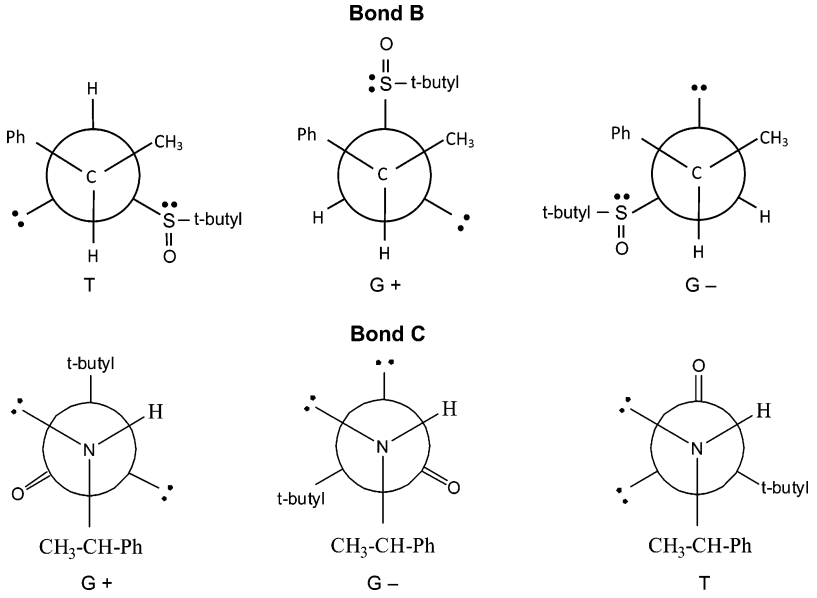

FIGURE 3. Newman projections around B and C bonds of **2** showing *trans* (T), plus *gauche* (G^+), and minus *gauche* (G^-) conformations.

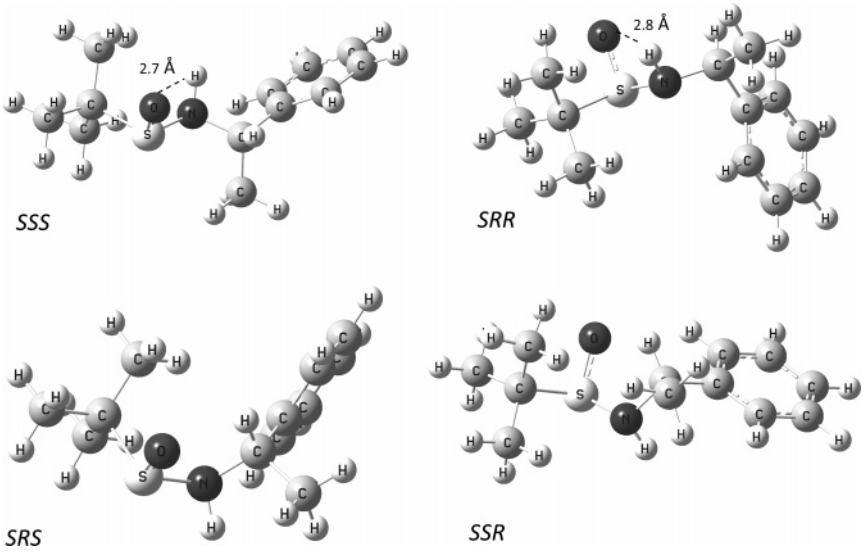

FIGURE 4. Four diastereomers, *SSS*, *SRR*, *SRS*, and *SSR*, of **2**. The three-letter designations represent configurational assignment at the stereogenic atoms C, N, and S, respectively. The remaining diastereomers are mirror images of these four. The conformation of each diastereomer shown is of lowest energy at the B3LYP/6-31G* level of theory.

influenced significantly in the presence of solvent. Therefore all calculations were done for **2**, as isolated molecule and solvent influence was not investigated. Exploration of the conformational space for each diastereomer was achieved by varying the dihedral angles corresponding to four rotatable bonds (A, B, C, and D in Figure 2). The conformational search was initiated with incremental 120° rotations around B and C bonds in order to obtain *trans* (T), plus *gauche* (G^+), and minus *gauche* (G^-) conformations. Newman projections of these conformations are given in Figure 3. The combination of T, G^+, and G^- conformations associated with the two dihedral angles has resulted in nine distinct conformations (TT, TG^+, TG^-, G^+T, G^+G^+, G^+G^-, G^-T, G^-G^+, G^-G^-). For each diastereomer, these conformers have been subjected to further geometry optimization. This further optimization has involved varying dihedral angles corresponding to bonds A and D (Figure 2). Since the bond A is associated with a planar phenyl ring, a 90° rotation was sufficient for conformational exploration. On the other hand, the *t*-butyl group associated with the bond D is C_3-symmetric, hence requiring only one 60° rotation for the conformational search.

Special attention was given to monitoring the configurational preference of nitrogen during the geometry optimization process because this chiral center is prone[23,24] to configurational inversion. As a result of nitrogen inversion during the optimization, some of the initial structures of *SRS*-**2** have converged into one of the stable conformations of *SSS*-**2**, and likewise some of the initial structures of *SSR*-**2** have converged into the stable conformations of *SRR*-**2**.

(23) Eliel, E. L.; Wilen, S. H. *Stereochemistry of Organic Compounds*; John Wiley & Sons, Inc: New York, 1994.
(24) Tanaka, M.; Aida, M. *Chem. Phys. Lett.* **2006**, *417*, 316−319.

TABLE 1. Fractional Populations for Stable Conformations of the Four Diastereomers of 2[a]

	configuration			
conformation	*SSS*	*SRR*	*SRS*	*SSR*
C_1	0.769	0.671	0.984	0.892
C_2	0.094	0.145	0.016	0.074
C_3	0.077	0.141		0.034
C_4	0.040	0.043		
C_5	0.012			
C_6	0.008			

[a] The populations are based on Gibbs free energies obtained with the B3LYP functional and the 6-31G* basis set.

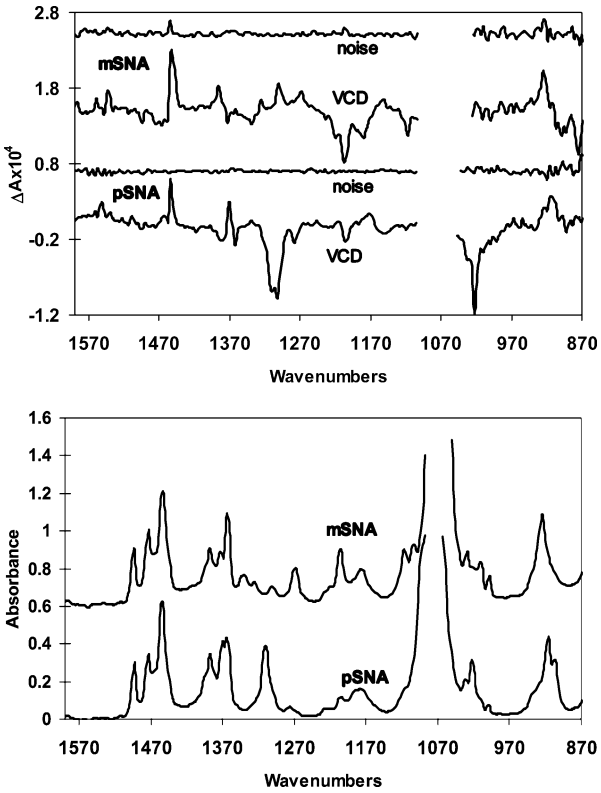

FIGURE 5. Experimental VA (bottom panel), VCD, and noise spectra for two diastereomers, *pSNA*-**2** and *mSNA*-**2**. VCD and noise traces are not shown in the region with excessive absorption intensity. The spectra of *mSNA* are shifted up for clarity.

The geometry optimization using the B3LYP functional and 6-31G* basis set has resulted in six stable conformations for *SSS*-**2**, four for *SRR*-**2**, two for *SRS*-**2**, and three for *SSR*-**2** diastereomers. The relative populations of the conformers of each diastereomer, determined from Gibbs free energies, are given in Table 1.

For each of the four considered diastereomers, the most stable conformer (labeled, C_1), is shown in Figure 4. All conformations identified as stable represent minima on the potential energy surface, as no imaginary vibrational frequencies have been predicted. Theoretical VCD, ECD, and ORD spectra for the stable conformations have been obtained using the same B3LYP functional and 6-31G* basis set. The comparison of population-weighted VCD, ECD, and ORD spectra for each of the eight diastereomers with the corresponding experimental data for two diastereomers (Figures 5−8) has indicated that *pSNA*-**2** corresponds to *SSS* configuration with six dominant conformations (C_1−C_6), and *mSNA*-**2** corresponds to *SRR* configuration with four dominant conformations (C_1−C_4). Figure 6A shows the correlation between the experimental spectra for *pSNA*-**2** and the B3LYP/6-31G* theoretical spectra for *SSS*-**2** (see Supporting Information for more details). Figure 6B displays corresponding correlation between the experimental VCD spectra of *mSNA*-**2** and the predicted VCD spectra for *SRR* configuration. Differences in the VCD band intensities among population weighted and experimental spectra could result from different sources: (a) the predicted relative intensities need not be accurate enough at the theoretical level used; (b) relative populations of conformers in solution environment used for experimental measurement can be different from that for an isolated molecule considered by the theoretical model.

The configurational assignment derived from VCD spectral analysis can be confirmed from a comparison between experimental and predicted ECD spectra. The negative ECD band at 209 nm for *pSNA*-**2** corresponds to the B3LYP/6-31G*-predicted negative ECD band at 213 nm (Figure 7A). On the other hand, the positive ECD of *mSNA*-**2** at 221 nm corresponds to the B3LYP/6-31G*-predicted positive ECD band at 242 nm (Figure 7B). Finally, a consideration of experimental and B3LYP/6-31G*-predicted ORD spectra also validates the VCD-based conclusion that *pSNA*-**2** corresponds to *SSS* configuration (Figure 8A), and *mSNA*-**2** corresponds to *SRR* configuration (Figure 8B); *pSNA*-**2** has positive optical rotation at all wavelengths measured, as does *SSS*-**2**. Similarly, *mSNA*-**2** has negative optical rotation at all wavelengths measured, as does *SRR*-**2**. It can be seen from Figures 6−8 that all three chiroptical methods exhibit agreement in the above-stated stereochemical assignments for the two experimentally considered diastereomers.

In the above analysis it should be noted that VCD spectral analysis of **2** is critical for the assignment of absolute configuration of diastereomers. Because of the presence of numerous vibrational transitions, comparison between experimental and predicted VCD spectra (Figure 6) allowed for distinguishing between different diastereomers, as only one diastereomer provides satisfactory match with the experimental VCD spectra. ECD spectral analysis (Figure 7), on the other hand, does not offer as much discrimination between different diastereomers because there is only one experimental ECD band in the accessible experimental region, and the sign of that one ECD band can be predicted for more than one diastereomer. In the case of *pSNA*-**2**, the one negative ECD band observed could be seen in the predicted spectra for *SSS*, *SRS*, and *SSR* diastereomers. In the case of *mSNA*-**2**, the one positive ECD band observed could be seen in the predicted spectra for *SRR*, *RRR*, *RSR*, and *RSR* diastereomers. Similarly, ORD spectral analysis (Figure 8) also does not offer as much discrimination between different diastereomers because the experimental optical rotations at all accessible wavelengths have a single sign, and that sign can be predicted for more than one diastereomer. In the case of *pSNA*-**2**, positive ORD has been predicted for *SSS*, *RSS*, and *RSR* diastereomers. In the case of *mSNA*-**2**, negative ORD has been predicted for *SRR*, *RRR*, *SSR*, and *SRS* diastereomers. Thus, while VCD spectral analysis of **2** provided the critical determination role, ECD and ORD spectral analyses of **2** provided a confirmatory role. In the chiroptical spectroscopic analysis of several diastereomers of a chiral molecule, VCD spectroscopy generally provides a better discriminatory role than ECD or ORD.

The dominant conformers of *SSS*-**2** and *SRR*-**2** are further examined by reoptimizing their geometries at a higher B3LYP/

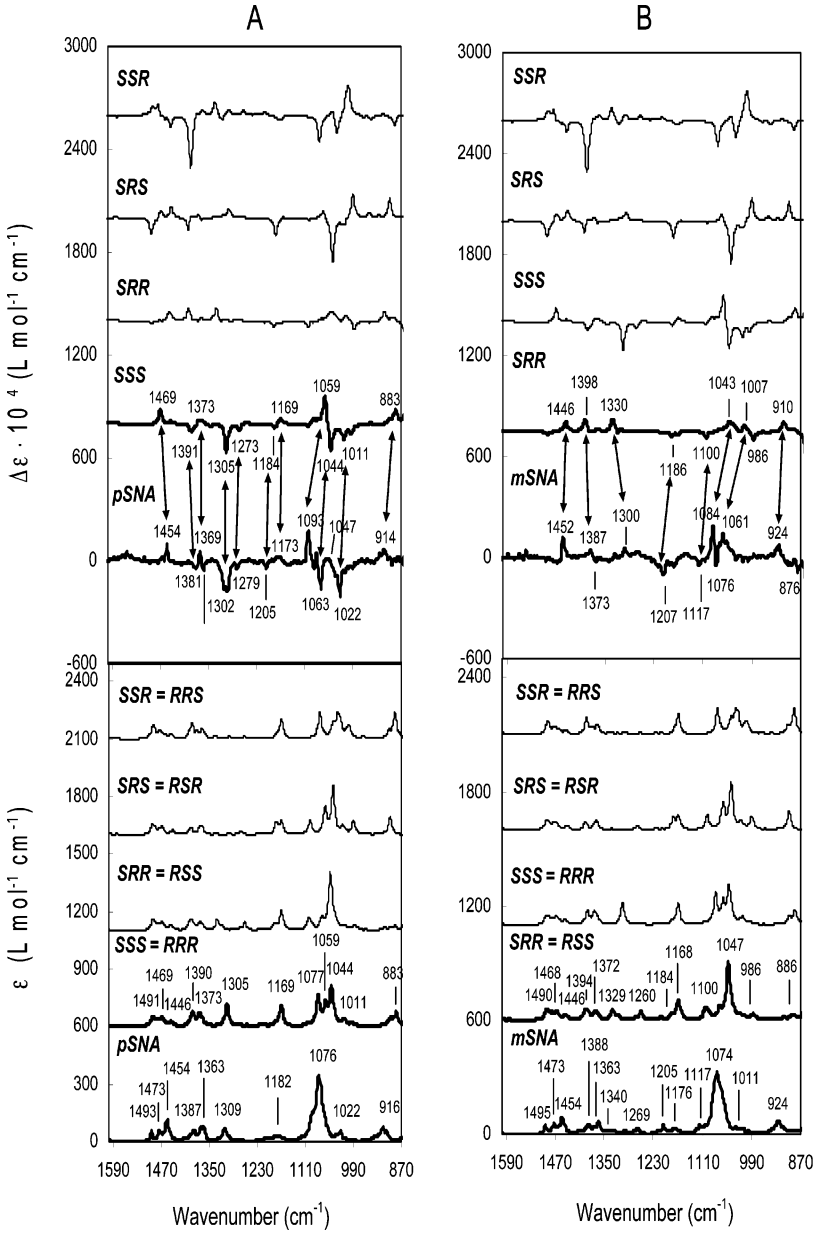

FIGURE 6. Comparison of the experimental VA and VCD spectra of *mSNA*-**2** and *pSNA*-**2**, with population-weighted spectra predicted for four diastereomers at the B3LYP/6-31G* level.

aug-cc-pVDZ level. These reoptimizations have resulted in the convergence of four conformations ($C_1'-C_4'$) each for *SSS*-**2** and *SRR*-**2**. The relative populations determined from Gibbs energies of the conformers determined at the B3LYP/aug-cc-pVDZ level are given in Table 2.

The B3YP/aug-cc-pVDZ-calculated vibrational absorption (VA) and VCD spectra of individual conformers along with the population-weighted spectra for *SSS*-**2** have been compared to the experimental spectra of *pSNA*-**2** in Figure 9. An analogous spectral comparison between *mSNA*-**2** and *SRR*-**2** is given in Figure 10. The double-headed arrows in these figures point to the correlated bands between the population-weighted VCD spectra of *SSS*-**2** and *SRR*-**2** and the experimental spectra of *pSNA*-**2** and *mSNA*-**2**, respectively (see Supporting Information for more details). The overall satisfactory correlation among multiple VCD bands at both theoretical levels (Figures 6 and 9) leads to the conclusion that *pSNA*-**2** has the *SSS* configuration, and *mSNA*-**2** has the *SRR* configuration. The vibrational assignments derived from B3LYP/aug-cc-pVDZ calculations are provided in the Supporting Information.

To confirm the configurational assignments derived from VCD spectral analysis, ECD and ORD spectra predicted at the higher B3LYP/aug-cc-pVDZ level are also considered. For this purpose the conformers with relative populations greater than 10% have been used. The spectral comparisons associated with ECD data are displayed in Figure 11, and that associated with ORD data are shown in Figure 12. In terms of the ECD spectra, *pSNA*-**2** displays an overall satisfactory qualitative agreement with the population-weighted spectra of *SSS*-**2**.

The negative experimental ECD band at 209 nm for *pSNA*-**2** corresponds to the B3LYP/aug-cc-pVDZ-predicted negative ECD band at 234 nm for *SSS*-**2** (Figure 11A). In terms of *mSNA*-**2**, its positive experimental ECD band at 221 nm corresponds to the B3LYP/aug-cc-pVDZ-predicted positive ECD band at

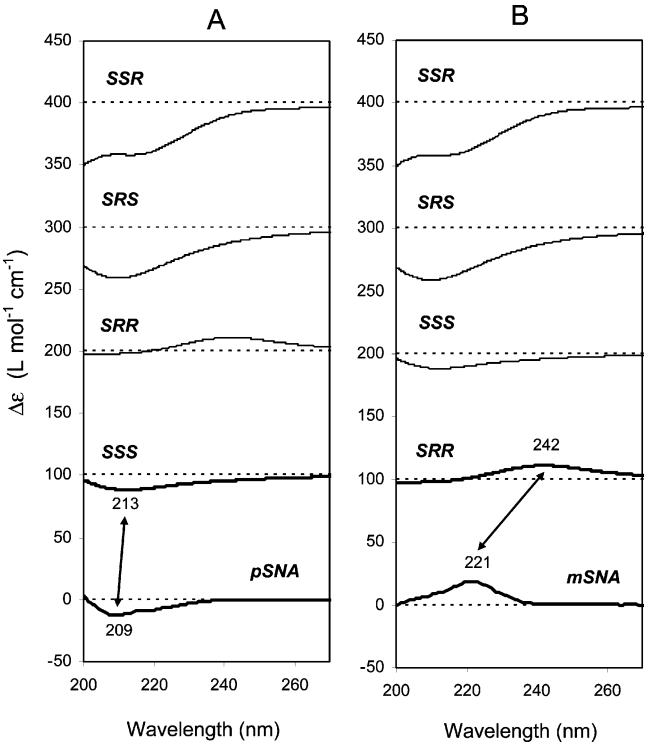

FIGURE 7. Comparison of the experimental ECD spectra of *mSNA*-**2** and *pSNA*-**2** with population-weighted spectra predicted for four diastereomers at the B3LYP/6-31G* level.

245 nm for *SRR*-**2** (Figure 11B). As noted in the study[21] of smaller sulfinamide **1**, it is not unusual for the electronic transitions predicted with the B3LYP functional to appear[25,26] at longer wavelengths than the experimentally observed transitions. With some blue shift of the predicted ECD bands, correlation between the positive ECD band of *mSNA*-**2** and the positive ECD band *SRR*-**2**, at both basis set levels, can be justified. Similarly, the correlation between the negative ECD band of *pSNA*-**2** and the negative ECD band of *SSS*-**2** at B3LYP/aug-cc-pVDZ level can be justified. The close positioning of the 6-31G*-predicted ECD band at 213 nm for *SSS*-**2** (Figure 7) with that of *pSNA*-**2** is most likely fortuitous.

TABLE 2. Fractional Populations for Stable Conformations of the *SSS* and *SRR* Diastereomers of 2[a]

	configuration	
conformation	*SSS*	*SRR*
C_1'	0.908	0.650
C_2'	0.043	0.173
C_3'	0.036	0.168
C_4'	0.014	0.009

[a] The populations are based on Gibbs free energies obtained with the B3LYP functional and the aug-cc-pVDZ basis set.

The absolute configurations derived from VCD and ECD spectral analyses are supported by a good qualitative agreement of ORD between experimental and B3LYP/aug-cc-pVDZ-predicted ORD spectra (Figure 12). The specific rotation signs for the population-weighted *SSS*-**2** remain positive at each of the six wavelengths considered, which is in agreement with that of *pSNA*-**2**. Likewise, specific rotation signs at all wavelengths considered for the population-weighted *SRR*-**2** remain negative as is the case for *mSNA*-**2** (see Supporting Information).

Satisfactory correlations between experimental and predicted spectra, from each of the three chiroptical spectroscopic methods, at both basis set levels, provide confidence to the conclusions established about the stereochemistry of diastereomers of **2**. They are fully supported by X-ray analysis carried out for the *mSNA*-**2** diastereomer. Crystal data, experimental details, and the basic geometric parameters are provided in the Supporting Information. The X-ray crystal structure of *mSNA*-**2** (Figure 13), which can be compared to the *SRR* diastereomer in Figure 4, unequivocally revealed that the absolute configura-

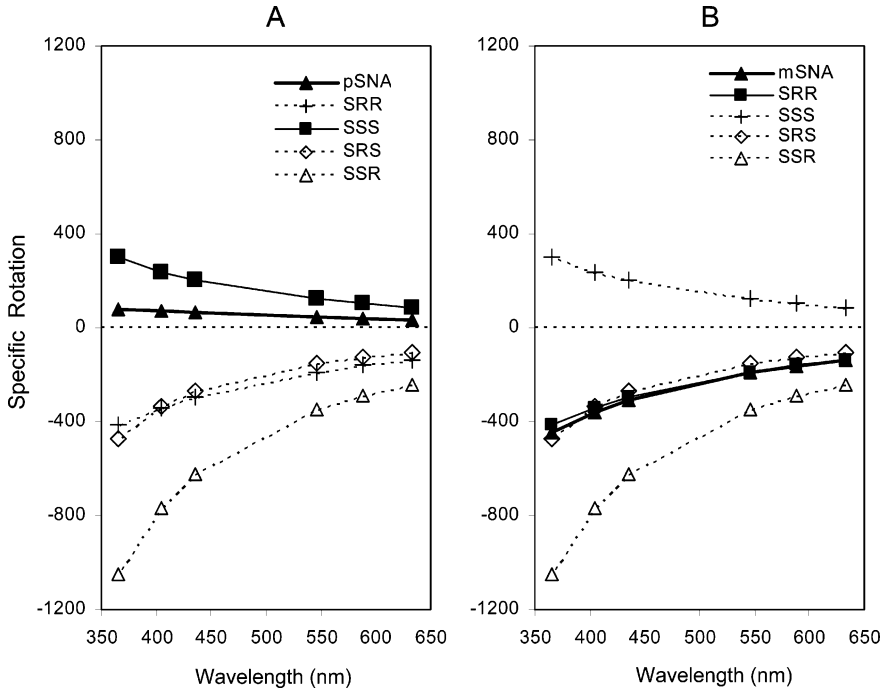

FIGURE 8. Comparison of the experimental ORD spectra of *mSNA*-**2** and *pSNA*-**2** with population-weighted spectra predicted for four diastereomers at the B3LYP/6-31G* level.

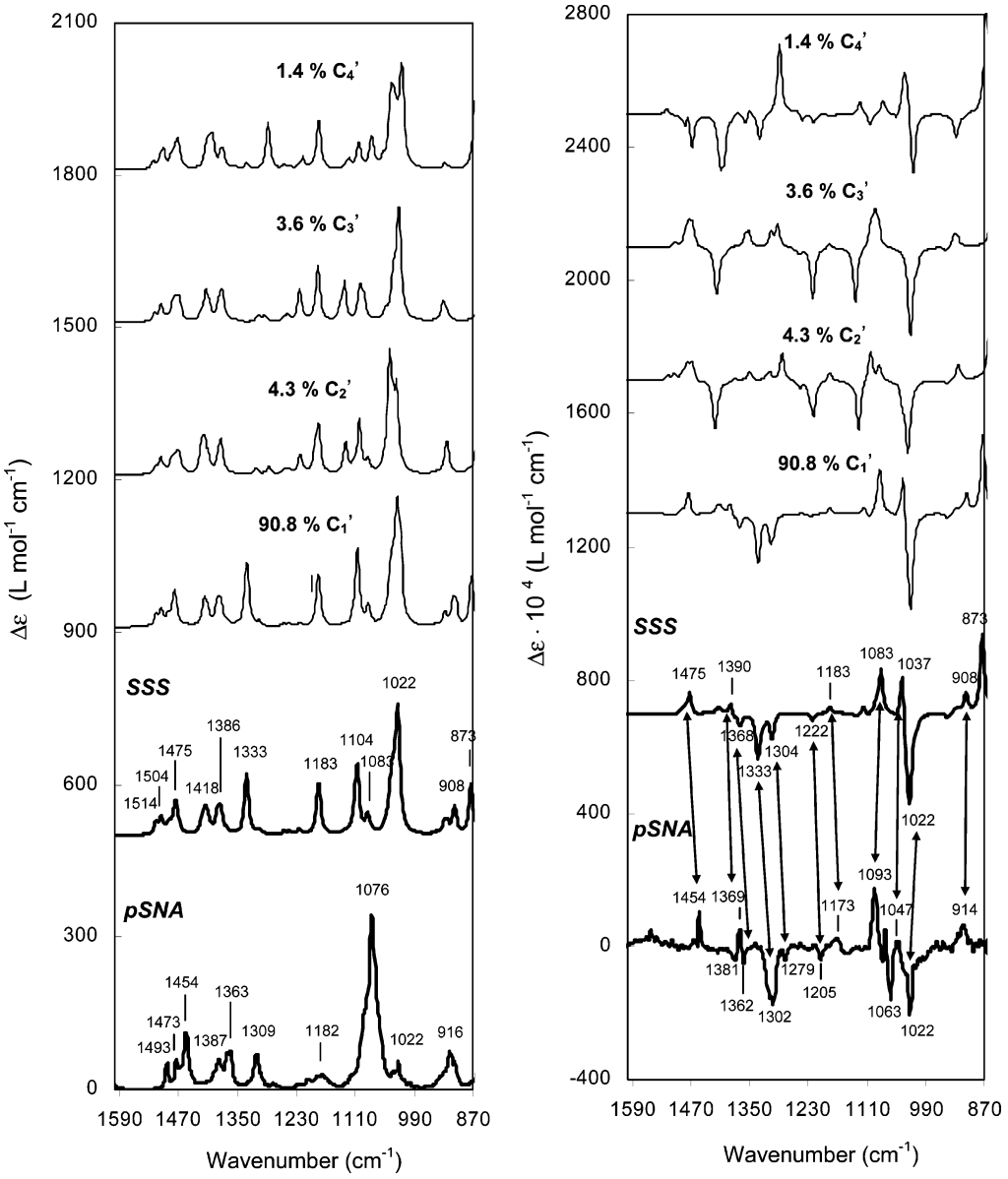

FIGURE 9. Comparison of the experimental VA and VCD spectra of *pSNA*-**2** with those predicted for *SSS*-**2** at the B3LYP/aug-cc-pVDZ level.

tions at the stereogenic carbon and sulfur atoms in *mSNA*-**2** are (*S*) and (*R*), respectively. The bond angles about the sulfur atom in the crystal structure are in the range 110.6(1)−98.6(1)°, and the assumed position of the lone pair of electrons indicates a distorted tetrahedral environment.

Finally, the sulfinamide diastereomer designated here as *mSNA*-**2** with (*S*)-absolute configuration at the C atom and (*R*)-absolute configuration at the S atom corresponds to the sulfinamide, designated as **5a** in ref 22a and sulfinamide **4c** in ref 22b. The sulfinamide diastereomer designated here as *pSNA*-**2**, with (*S*)-configurations at both C and S atoms has not been reported before, but the one with (*R*)-configurations at both C and S atoms has been reported as **4a** in ref 22a.

Conclusion

On the basis of the experimental and density functional theory (DFT)-predicted VCD spectra, the absolute configurations and dominant conformations for two diastereomers of *N*-phenylethyl-*t*-butylsulfinamide (**2**) have been determined. One diastereomer, *pSNA*-**2** has the *SSS* configuration with one predominant conformation, while the second diastereomer *mSNA*-**2** has the *SRR* configuration with three predominant conformations. These conclusions are supported by the ECD and ORD spectral analyses and also by the X-ray analysis carried out for *mSNA*-**2**.

Experimental Section

The Dextrorotatory and Levorotatory Diastereomers of *N*-α-Phenylethyl-*t*-butylsulfinamide, *pSNA*-2 and *mSNA*-2. A solution of (*S*)-(−)-α-phenylethylamine (2.45 g, 20 mmol) and triethy-

(25) Bauernschmitt, R.; Ahlrichs, R. *Chem. Phys. Lett.* **1996**, *256*, 454−464.
(26) Polavarapu, P. L.; He, J.; Jeanne, C.; Ruud, K. *Chem. Phys. Chem.* **2005**, *6*, 2535−2540.

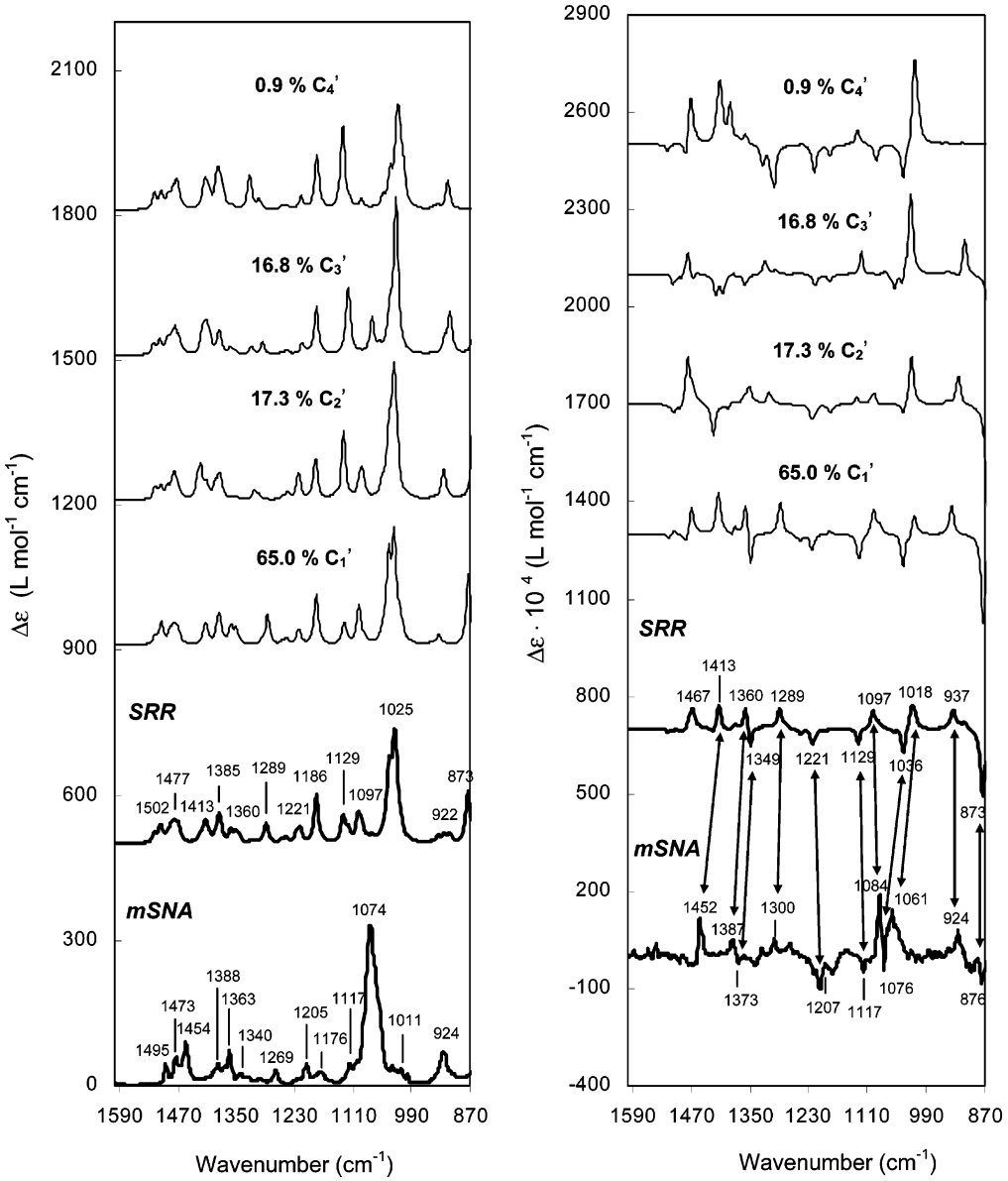

FIGURE 10. Comparison of the experimental VA and VCD spectra of *mSNA*-**2** with those predicted for *SRR*-**2** at the B3LYP/aug-cc-pVDZ basis level.

lamine (2.2 g, 22 mmol) in Et_2O (10 mL) was added dropwise with vigorous stirring to a solution of *t*-butanesulfinyl chloride (2.8 g, 20 mmol) in Et_2O (100 mL) at −70 °C. After the reaction mixture was stirred for 6 h at −70 °C and 72 h at room temperature, the solution was diluted with diethyl ether (50 mL) and quenched with water. The organic phase was separated and washed with 5% H_2SO_4 solution, 5% K_2CO_3 solution, and water and dried over $MgSO_4$. After the solvent was removed under reduced pressure, the crude sulfinamide (4.35 g) was purified by column chromatography on silica gel (110 g). The column was washed subsequently with petroleum ether/diethyl ether [1:1 v/v (86 × 10 mL)] and diethyl ether (43 × 10 mL). Evaporation of petroleum ether/diethyl ether (1:1) fractions 41−56 gave the pure dextrorotatory diastereomer (0.52 g) with $[\alpha]_{589} = +41.3$ ($c = 1.55$, $MeCO_2Et$). Oil: Anal. Calcd. for $C_{12}H_{19}NOS$: C, 63.94; H, 8.50; N, 6.22; S, 14.24. Found: C, 63.81; H, 8.73; N, 6.53; S, 14.64. Evaporation of petroleum ether/diethyl ether (1:1) fractions 21−40 gave another oil sample of the dextrorotatory diastereomer (2.2 g) with $[\alpha]_{589} = +39.65$ ($c = 1.16$, $MeCO_2Et$), the ^1H NMR of which was identical to that of the first sample. Evaporation of diethyl ether fractions 11−43 gave the pure levorotatory diastereomer (0.978 g) with $[\alpha]_{589} = -91.0$ ($c = 1.24$, $MeCO_2Et$); white solid mp = 70 °C.

Spectral Measurements. The VA and VCD spectra were recorded in the 2000−870 cm^{-1} region using a Fourier Transform VCD spectrometer modified[27] to reduce the level of artifacts. The spectra of *pSNA* and *mSNA* were obtained with 3 h data collection time, at 4 cm^{-1} resolution, in a variable path length cell with BaF_2 windows. Measurements were done in CCl_4 solvent. Solvent absorption has been subtracted from the presented absorption spectra. The enantiomers or racemic mixtures of the studied diastereomers are not available, and therefore the VCD spectra of solvent were subtracted from those of the samples.

The experimental VA, VCD, and noise spectra for *pSNA*-**2** measured at 0.189 M concentration with 300 μm path length are shown in Figure 5. Those for *mSNA*-**2**, measured at 0.343 M concentration with 200 μm path length are also shown in Figure 5. In these spectra, the ∼1030−1103 cm^{-1} region is not shown

(27) Shanmugam, G.; Polavarapu, P. L. *J. Am. Chem. Soc.* **2004**, *126*, 10292−10295.

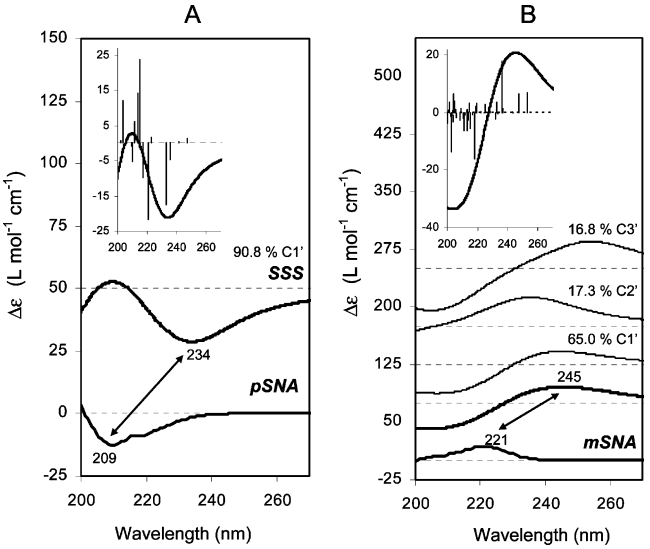

FIGURE 11. Comparison of experimental and B3LYP/aug-cc-pVDZ theoretical ECD spectra of **2**. The inset shows the calculated spectrum with the location of individual electronic transitions and their ECD intensities.

because of the excessive absorbance in this region. Separate measurements, at 0.175 M concentration and 140 μm path length for *pSNA*, and at 0.138 M concentration and 170 μm path length for *mSNA*, were undertaken to measure the absorption and associated VCD signals in this missing region. These two separate measurements have been combined to compare the experimental spectra in the entire region of the measurement with the predicted spectra.

The concentration-dependent VA spectra of **2** have also been measured (not shown) in CCl_4 solvent, in the concentration range of ~77−15 mg/mL (0.343−0.067 M), to examine the presence of dimers. However, no evidence of dimer formation was apparent for either diastereomer.

The ECD spectra were recorded using a 0.01 cm path length quartz cell. The concentrations used were 0.0195 M for *pSNA* and 0.0213 M for *mSNA* in hexane. The optical rotations at six discrete wavelengths (633, 589, 546, 436, 405, and 365 nm) were measured with a 1 dm cell. The concentration-dependent ORD measurements for **2** were obtained in the concentration ranges 38.6×10^{-3} to 3.0×10^{-4} g/mL (0.0865−0.0006 M) for *pSNA*-**2**, and 19.5×10^{-3} to 1.5×10^{-4} g/mL (0.1713−0.0013 M) for *mSNA*-**2**. The concentration-dependent specific rotations have been extrapolated to zero concentration to determine[28] the intrinsic rotations. The experimental ORD data presented here correspond to these intrinsic rotations.

Calculations. Geometry optimizations and chiroptical spectroscopic predictions for **2** were undertaken with quantum mechanical programs[29,30] using DFT and the B3LYP functional. The previous investigation on **1** revealed[21] that calculations with the smaller 6-31G* basis set with the B3LYP functional are not adequate for obtaining reliable predictions of electronic properties for **1**. On the other hand, calculations with the larger aug-cc-pVDZ basis set with the B3LYP functional were found[21] to provide a consistent stereochemical assignment. Guided by these earlier results, both 6-31G* and aug-cc-pVDZ basis sets were used for the calculation of chiroptical spectroscopic properties of **2**.

The theoretical absorption and VCD spectra of **2** were simulated with Lorentzian band shapes and a 5 cm^{-1} half-width at 1/2 of peak height. Frequencies calculated at the B3LYP/ 6-31G* level were scaled by a factor of 0.9613. Frequencies obtained at the B3LYP/aug-cc-pVDZ level have not been scaled.

The theoretical ECD spectra of **2** were simulated from the first 30 singlet → singlet electronic transitions using Lorentzian band shapes and a 20 nm half-width at 1/2 of peak height. Rotational strength values, calculated with velocity representation, have been used for the ECD spectral simulations. The predicted ECD intensities of **2** have been scaled-up by a factor of 6 in order to facilitate a qualitative comparison with the experimental ECD spectra.

Crystal and Molecular Structure of the Levorotatory Diastereomer of *N*-α-Phenylethyl-*t*-butylsulfinamide, mSNA-2. (A) Crystal data for *mSNA*-2. $C_{12}H_{19}NOS$, colorless, plate 0.22 × 0.15 × 0.07 mm, orthorhombic, space group $P2_12_12_1$, $a = 5.7913$ (19), $b = 12.976$ (3), $c = 17.478$ (4) Å, $V = 1313.4$ (6) Å,^{3} $M_r = 225.35$, $Z = 4$, $d_{calcd} = 1.140$ g cm^{-3}, $\mu = 1.99$ mm^{-1}, $T = 296$ (2) K, $F(000) = 488$.

(B) Data Collection. Enraf-Nonius CAD-4 diffractometer with graphite monochromatized Cu Kα radiation. Measured reflections 3051 (θ_{max} 75.0°), 2699 independent (R_{int} 0.074).

(C) Structure Solution. direct method, anisotropic refinement on F^2 for all non H atoms, while H atoms were generally fixed in idealized positions (with the exception of some N−H protons, whose positions were determined from a difference map) and refined with their displacement parameters riding on those of their parent atoms. The structure was refined over 2654 reflections with $I > 2\sigma(I)$ (145 refined parameters with 18.3 reflections on parameter). The correct absolute structure was proved by Flack parameter[31] $x = 0.00(2)$. For all data, the final $wR2$ was 0.131, $R1 = 0.048$, $S = 1.08$, max $\Delta\rho = 0.56$ e Å^{-3}. Data processing was carried out with the CAD-4 Manual[32] and SDP;[33] structure solution SHELXS;[34] structure refinement SHELXL.[35] Full details (excluding

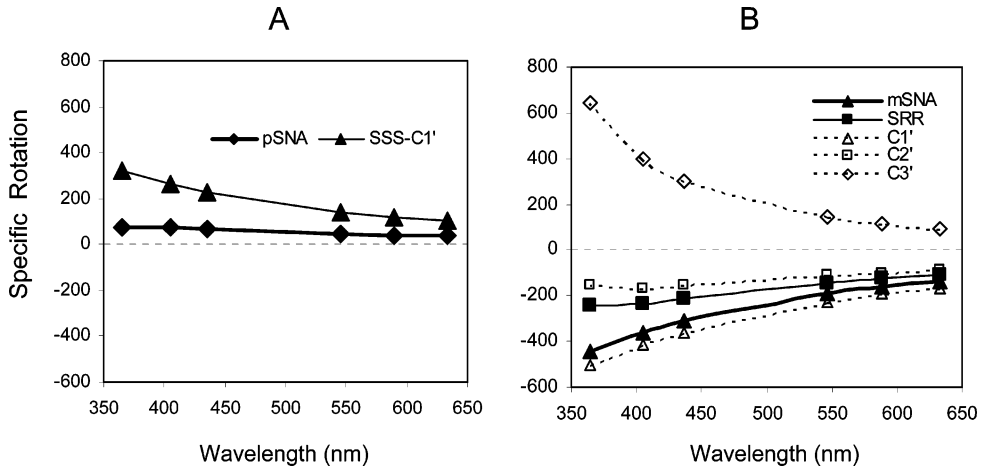

FIGURE 12. Comparison of the experimental and B3LYP/aug-cc-pVDZ theoretical ORD spectra of **2**.

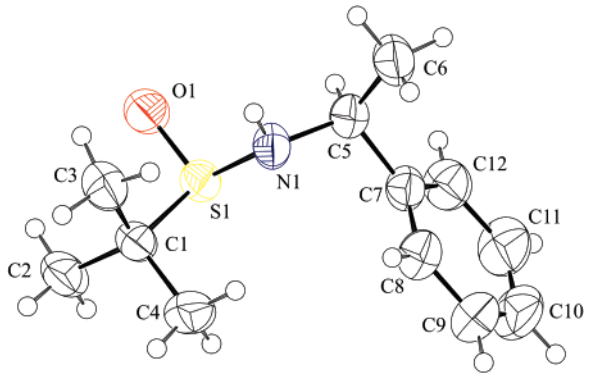

FIGURE 13. The molecular structure of *mSNA*-**2** determined from X-ray diffraction data, showing 50% probability ellipsoids.

the structure factors) for the structure have been deposited at the Cambridge Crystallographic Data Center, as supplementary publication no. CCDC 669314 and can be obtained free of charge upon application to CCDC, 12 Union Road, Cambridge CB2 1EZ, U.K. [e-mail: deposit@ccdc.cam.ac.uk].

Acknowledgment. Computational work was partially supported by the National Center for Supercomputing Applications under TG-CHE060063T and utilized the NCSA IBM P690 and SGI Altix systems. Teaching assistantship from Vanderbilt University (to A.G.P.) is greatly appreciated. The studies in Lodz were in part financially supported (as Grant PBZ-KBN-126/TO9/02 for J.D.) in the frame of a scientific project by the government fund created to support science in the 2006−2009 period.

Supporting Information Available: General experimental information, correlation between experimental and predicted VCD bands, vibrational assignments, correlation between experimental and predicted ORD data, tables of Cartesian coordinates and energies of different conformers of **2** at B3LYP/aug-cc-pVDZ level, tables of X-ray data, a figure showing intermolecular hydrogen bonding in the crystal structure, and proton NMR spectra. This material is available free of charge via the Internet at http://pubs.acs.org.

JO702544G

(28) Polavarapu, P. L.; Petrovic, A. G.; Wang, F. *Chirality* **2003**, *15*, S143−S149.
(29) *Gaussian 98*; Gaussian, Inc.: Pittsburgh, PA, 1998 (full citation is given in the Supporting Information).
(30) *Gaussian 03*; Gaussian, Inc.: Wallingford, CT, 2004 (full citation is given in the Supporting Information).
(31) Flack, H. D. *Acta Crystallogr., Sect. A* **1983**, *39*, 876−881.
(32) Schagen, J. D.; Straver, L.; van Meurs, F.; Williams, G. *CAD-4 Manual*; Data collection program; Enraf-Nonius: Delft, The Netherlands, 1989.
(33) Frenz, B. A. *SDP*; Data reduction program; Enraf-Nonius: Delft, The Netherlands, 1986.
(34) Sheldrick, G. M. *SHELXS97*; University of Göttingen: Göttingen, Germany, 1997.
(35) Sheldrick, G. M. *SHELXL97*; University of Göttingen: Gottingen, Germany, 1997.